Thermal stress analysis and fatigue strength measurement of the interface between concrete and polymer cement mortar

T. Matsumoto & T. Mahaboonpachai
Department of Civil Engineering, University of Tokyo, Tokyo, Japan

Y. Inaba
Kajima Technical Research Institute, Kajima Corporation, Tokyo, Japan

R. Rumbayan
Polytechnic of Manado, Manado, Indonesia

ABSTRACT: This paper mentions two major studies on the delamination of external wall tile structures. External wall tile structures are usually made of tile, adhesive mortar, and concrete, and the interfaces between layers are considered to be a weak location against delamination. First, from the viewpoint of reaction, the heating experiment of a small scale tile structure was conducted. The temperature distribution in the through-thickness direction was measured with a thermography, and, based on the measured temperature, the stresses at the interface are estimated with simple analytical models. Next, from the viewpoint of resistance, the measurement of interfacial fracture energy and fatigue strength between concrete and polymer cement mortar were carried out. The interfacial bond strengths and their S-N diagrams are obtained. Based on the studies of reaction and resistance, the mechanisms of interfacial failure observed in external wall tile structures are discussed in order to achieve the durability of the interface and the tile structures.

1 INTRODUCTION

This paper mentions preliminary studies under a research program that has been conducted for the purposes of understanding the mechanisms of interfacial failure observed in external wall tile structures and achieving the durability of the interface and the tile structures.

The external wall tile structure of a building is composed of three different materials: ceramic tiles, adhesive mortar, and concrete. Therefore, bi-material interfaces are inevitable in the tile structure. Under service conditions, these interfaces are subjected to environmental actions such as temperature cycles, dry and wet cycles, UV radiation, chemical pollutants, and so on, and it is observed that the interfaces are the location where the failure of the tile structure initiates (Kumagai 1991).

Among these environmental actions, temperature cycles, which lead to the cycles of interfacial stresses in the normal and shear direction, are considered to be important. If these interfacial stresses are significant compared to their static strength, it is possible that interfacial delamination takes place and its fatigue propagation leads to the failure and fall-off of the tile structure. Therefore, in order to understand the mechanisms of interfacial failure, the current study conducts the thermal stress analysis of the interface via temperature measurement with a thermography, and also conducts the experimental measurement of interfacial fracture energy under static loading and of fatigue strength under fatigue loading. Namely, these studies are conducted in order to clarify the "reaction" and "resistance" of the interface in the tile structure

First, the heating experiment of a tile structure will be explained. The experiment was carried out in order to obtain the temperature distribution of a tile structure in the thickness direction. Using the measured temperature distribution, thermally induced interfacial stresses are calculated based on simple analytical models.

Next, the fracture energy and the fatigue strength measurement of the bi-material interface between concrete and polymer cement mortar will be explained. Based on interfacial fracture mechanics, bi-material interface specimens were tested under the mixture of normal and shear stress, and the interfacial fracture energy was measured by taking into account the mismatch parameters of two materials. The interfacial fracture energy is also analyzed with finite element analysis so that the tensile and shear bond strengths can be calculated. Furthermore, the fatigue test was carried out for the same type of bi-material interface specimens in order to grasp the fatigue strength characteristics in terms of S-N diagrams.

Finally, based on the thermal stress estimate as reaction and the bond strengths and the S-N diagrams as resistance, the possible failure mechanisms of the bi-material interface in the tile structures will be discussed.

2 THERMOGRAPHIC MEASUREMENT OF THE TILE STRUCTURE AND THERMAL STRESS ANALYSIS AT THE INTERFACE

First, this chapter explains the thermographic measurement of temperature distribution of the tile structure under monotonic thermal loading, where the thermal loading was given simulating the real building environmental conditions.

Second, in this chapter, using the measured temperature distribution, thermal stresses at the interface are estimated based on simple analytical models for shear and normal stress.

2.1 *Material and specimen*

The tile structure is made of three layers: concrete substrate, adhesive mortar, and tiles. A small scale specimen was fabricated for the current measurement purpose (Figure 1). The specimen has the thickness of 110 mm, and its tile surface side has the area of 200 mm by 100 mm.

The concrete layer of the specimen is made of normal strength concrete. The adhesive mortar of the current experiment is polymer cement mortar, the mix proportion of which is given in Table 1. The thickness of the adhesive mortar is 5 mm, which
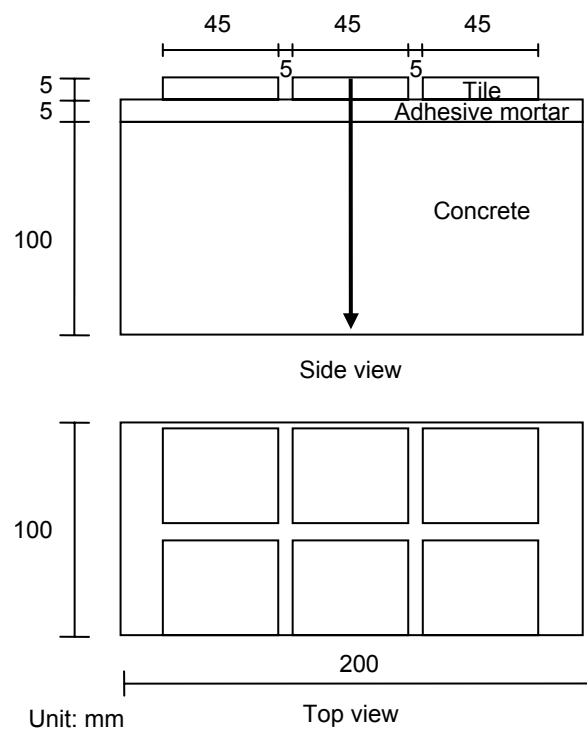
Figure 1. Specimen geometry and dimensions. The arrow shows the line along which the surface temperature is measured.

Table 1. Mix composition of adhesive mortar. W: water, C: cement, S: sand, P: Ethylene-vinyl acetate copolymer, MC: Methylcellulose (kg/m^3).

S/C	W/C	W	C	S	P	MC
50	30	335	1117	559	45	1.69

is commonly used in practice. The tiles are glazed porcelain with gray color, and they are 45 mm in length and width and 5 mm in thickness.

First, the adhesive mortar was mixed with water by hoe until achieving buttery consistency. Secondly, the fresh adhesive mortar was applied on a concrete plane. After five minutes of opening time, the glazed porcelain tiles were laid in. The open time may lead to reducing the wettability and also make the fresh adhesive mortar more effective in spreading over. Finally, the specimen was stored for 28 days at room temperature before thermographic temperature measurement.

Since the specimen has to represent a real tile structure in a building where heat flows only in the wall through-thickness direction, the four side surfaces of the specimen were covered by a heat insulation material. The heat insulation material is made of glass wool, and it prevents the heat from neither entering nor leaving the specimen. This was confirmed by comparing the heating experiment with and without the heat insulation. The results showed that the current heat insulation was satisfactory enough to achieve its purpose.

2.2 *Heating experiment*

Monotonic thermal loading was applied to the tile surface of the specimen by using two lamps. The tile surface of the specimen was heated from room temperature, about 29 degrees Celsius, up to around 50 degrees Celsius, and the measurement of temperature distribution was done with a thermography.

For the thermographic measurement, one side of the heat insulation material was opened for five seconds (the side shown in Figure 1), and the measurements were carried out at the interval of ten minutes, so that the heat loss could be minimized.

For the justification of these measurement procedures, a measurement was carried out without opening the side until the tile surface reached 50 degrees Celsius, and its result was compared with that of the current method. The difference of the measured temperature was less than 1 degree Celsius. This implies that the error of the current method is less than around 2 %, and also supports that the measurement on the side surface substitutes that of inside specimen.

Figure 2 shows the thermal image of the specimen side surface at 40 minutes after heating. It shows uniform enough temperature distribution horizontally. The thermographic measurements were done before heating was applied, and at 5, 10, 20, 30, and 40 minutes. At 40 minutes, heating was stopped, and the measurements were continued at 10 and 20 minutes after heating was stopped.

Figure 3 shows the temperature profile on the side surface of the specimen in the thickness direction (along the arrow in Figure 1). Before heating,

the temperature was around 28.5 degrees Celsius through the thickness. It can be observed that the tile surface temperature quickly increased up to 37 degrees Celsius at 5 minutes after heating was applied. From 5 to 40 minutes, the temperature of concrete increased due to the heat conduction. At 40 minutes, the heating was stopped, and soon the tile temperature dropped from 48.6 to 41.2 degrees Celsius. By 20 minutes after the stop of heating, the heat conduction took place in the reverse way, resulting in the temperature decrease of concrete on the tile surface side.

For the later thermal stress analysis, the average temperature of each layer, i.e. tile, adhesive mortar, and concrete, is calculated and plotted with time in Figure 4. Also, the temperature at both sides of the tile is plotted with time in Figure 5. In Figure 4, it is seen that the temperature difference is more significant between adhesive mortar and concrete, and, in Figure 5, the maximum difference between both sides appears at 5 minutes, although it is rather small. These figures will be used for shear and normal stress estimate in the next section, respectively.

2.3 Analytical models for thermal stress analysis

Stresses arise at the interfaces due to the mismatch of elastic and thermal properties of three layers. In this section, shear and normal stress are estimated by using simple analytical models proposed by Kumagai (1994).

The shear stress model consists of three linear elastic materials: tile, adhesive mortar, and concrete (Figure 6). The main assumptions of the model are no bending moment and no shear deformation in tile and concrete.

The shear stress, τ, can be expressed as

$$\tau = \frac{C(\alpha_1 T_1 - \alpha_2 T_2)}{\left(\dfrac{1}{E_1 t_1} + \dfrac{1}{E_2 t_2}\right) cosh \dfrac{\beta_s}{2}} sinh \frac{\beta_s x}{L} \tag{1}$$

where α_1 = thermal expansion coefficient of concrete; α_2 = thermal expansion coefficient of tile; T_1 = average temperature of concrete; T_2 = average temperature of tile; E_1 = Young's modulus of concrete; E_2 = Young's modulus of tile; t_1 = thickness of concrete; and t_2 = thickness of tile. C and β_s are given as follows:

$$\beta_s = C \times L = \sqrt{\frac{G}{t_3}\left(\frac{1}{E_1 t_1} + \frac{1}{E_2 t_2}\right)} \times L \tag{2}$$

where G = shear modulus of adhesive mortar which can be obtained with E = Young's modulus of adhesive mortar and ν = Poisson's ratio of adhesive mortar and where t_3 = thickness of tile and L = the

longer side length of tile. Details of the derivation can be found elsewhere (Kumagai 1994).
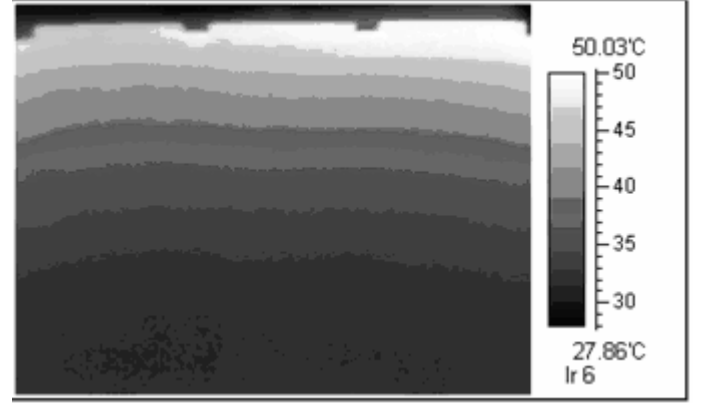
Figure 2. Thermal image of the specimen side surface at 40 minutes after heating.
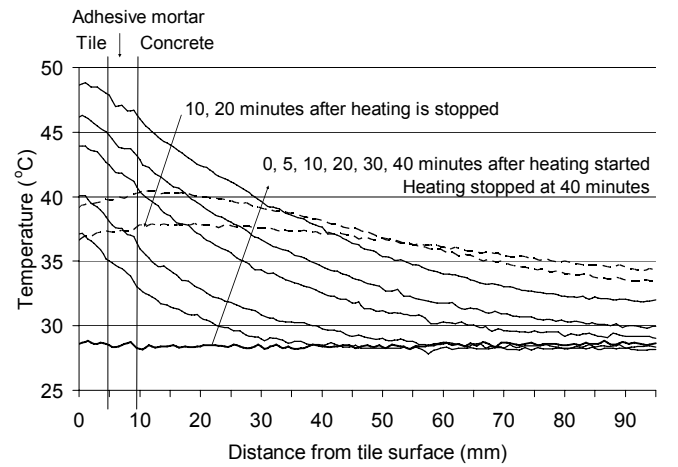
Figure 3. Temperature profile in the tile structure in the thickness direction.
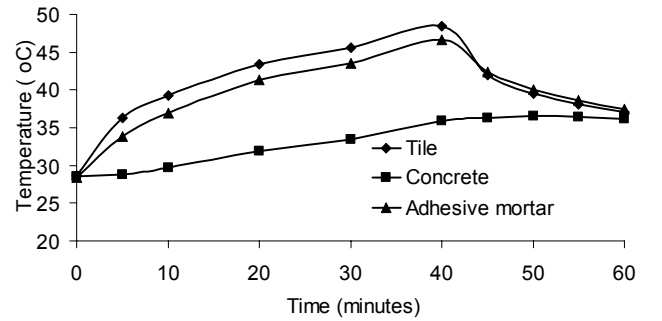
Figure 4. Average temperature of each layer.
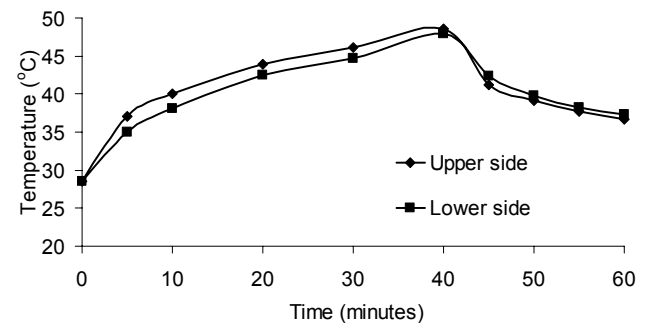
Figure 5. Tile temperature at both sides.

The normal stress model consists of two layers: tile and lamped layer of adhesive mortar and concrete (Figure 7). It is assumed that the adhesive is very thin compared to concrete thickness and that no bending exists in concrete, meaning that tile bends over elastic foundation.

The normal stress, σ, can be expressed as

$$\sigma = yK \tag{3}$$

where

$$y = \frac{\cosh \beta_n x \cos \beta_n x + \phi \sinh \beta_n x \sin \beta_n x}{2\beta_n^2 \left(\sinh \dfrac{\beta_n L}{2} \sin \dfrac{\beta_n L}{2} - \phi \cosh \dfrac{\beta_n L}{2} \cos \dfrac{\beta_n L}{2} \right)} \tag{4}$$

$$\frac{\alpha_2 \Delta T_2}{t_2}$$

and

$$\phi = \frac{\sinh \dfrac{\beta_n L}{2} \cos \dfrac{\beta_n L}{2} + \cosh \dfrac{\beta_n L}{2} \sin \dfrac{\beta_n L}{2}}{\sinh \dfrac{\beta_n L}{2} \cos \dfrac{\beta_n L}{2} - \cosh \dfrac{\beta_n L}{2} \sin \dfrac{\beta_n L}{2}} \tag{5}$$

ΔT_2 is temperature difference between upper and lower side of tile. Furthermore, K is normal stiffness of the lamped layer per unit length and can be obtained as

$$K = \frac{E_1}{mLd_2 \left(1 - \upsilon_1^2 \right)} \tag{6}$$

where d_2 is the shorter side length of tile and m is tile shape coefficient, which is equal to 0.95 for square shape. Again, details can be found elsewhere (Kumagai 1994).

2.4 *Thermal stress analysis*

Using the temperature distribution by a thermography and material properties in Table 2, shear and stress distribution is plotted with time in Figure 8, and normal stress distribution in Figure 9.

It is observed that the maximum shear stress occurs always at the edge of the tile. The shear stress rapidly increases up to 20 minutes, and slowly increases after 20 minutes. This coincides with the temperature distribution in Figure 4. Namely, the temperature difference between tile and concrete produces the shear stress in the observed way. Heating was stopped at 40 minutes, and the observation continued up to 20 minutes after heating stopped. The decrease of the shear stress after 40 minutes is fast, again in relation to the decrease of the temperature difference between tile and concrete. During the observation, the maximum shear stress is estimated to be 2.625 MPa for the tile surface temperature 48.64 degrees Celsius.

For the normal stress, the maximum value in compression is observed at the edge of the tile, while the maximum value in tension is at the center of the tile. Both maximum values happen at 5 minutes.
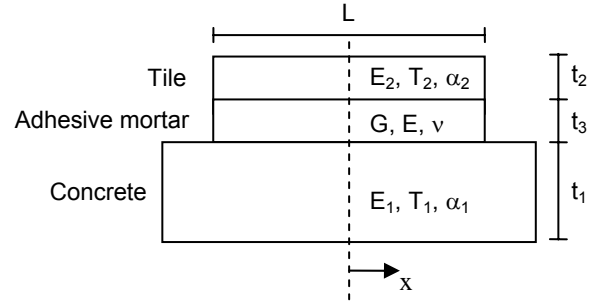
Figure 6. Shear stress model.
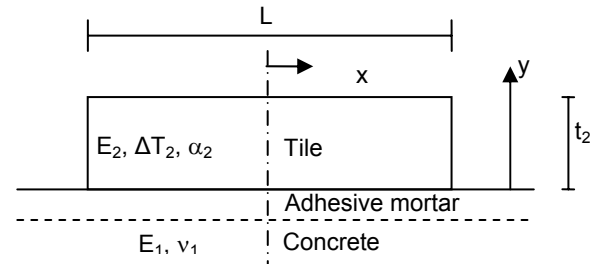
Figure 7. Normal stress model.
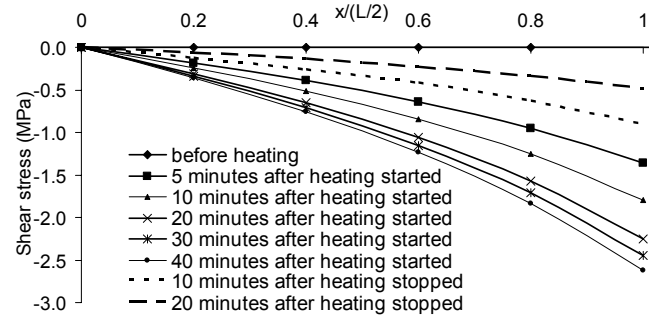
Figure 8. Shear stress distribution.
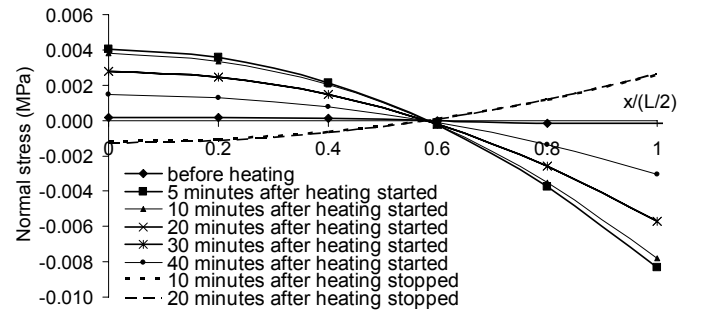
Figure 9. Normal stress distribution.

Table 2. Material properties.

	Concrete	Adhesive mortar	Tile
Young's modulus (GPa)	30.7	21.6	80.0
Poisson's ratio	0.207	0.212	-
Thermal expansion coefficient (/^{o}C)	0.000006	-	0.000008

This again coincides with the temperature difference between both sides of the tile, which can be seen in Figure 5. Heating increases the temperature difference up to 5 minutes, but it soon decreases the difference after 5 minutes. Following this behavior, the normal stress becomes close to zero along the interface at 40 minutes. Furthermore, the stress direction changes after 40 minutes, meaning that the tile bends upwards. This is due to the fact that the lower side of the tile becomes hotter than the upper side in cooling process, as is seen in Figure 5. During the observation, the maximum normal stress is estimated to be 0.008 MPa in compression at the edge and 0.004 MPa in tension at the center. Both happen at 5 minutes for the tile surface temperature 37.12 degrees Celsius.

Although it has to be admitted that the current simple models have a lack of accuracy due to their assumptions and that a more rigorous analysis such as finite element analysis is necessary to analyze this kind of crack problem, the current models together with thermographic measurement yield the estimate of interfacial stresses under thermal loading. It estimate the shear stress on the order of 1 MPa and the normal stress on 10^{-3} MPa. The interface is subjected more severely to shear stress, if we assume the strengths in shear and normal are also on the order of 1 MPa. With this estimate of stresses and the fatigue strength characteristics

3 MEASUREMENT OF FRACTURE ENERGY AND FATIGUE STRENGTH OF BI-MATERIAL INTERFACE

3.1 *Determination of interfacial fracture energy under mixed mode fracture*

The evaluation of bond at the interface is usually made either in tension or flexure.

The tensile bond test is common, and is widely used for the evaluation of the interfacial bond strength evaluation between adhesive mortar and concrete (Austin et al. 1995). The interfacial bond is evaluated as tensile bond strength of the bonded area.

The evaluation method in flexure is also reported (Kunieda 2000). In this method, beam specimens made of two kinds of materials are fabricated, and a notch is introduced at the bi-material interface (Figure 10). The beam specimens are loaded under four point flexure, and the observed interfacial fracture is treated as a mode I fracture problem. Therefore, the interfacial bond is evaluated in terms of fracture energy and bridging stress-crack opening displacement relation.

The current study aims at the evaluation of interfacial fracture under the combination of tension and shear stress, since the bi-material interface of a tile structure is subjected to the various combination of tension and shear stress depending on the environmental conditions. Hence, in addition to symmetric four point loading in Figure 10, asymmetric four point loading in Figure 11 was applied.

Under the mixture of tension and shear stress, the interfacial fracture has to be treated as a fracture under the combination of mode I and II, and the interfacial fracture energy is expressed as a function of phase angle, which represents the relative proportion of shear to normal stress at the interface.

Following O'Dowd (1992), interfacial fracture energy, Γ, and phase angle, ψ, can be calculated as follows:

$$\Gamma(\psi) = \frac{1-\beta^2}{E_*}\left|K_c^2\right| \quad \text{and} \tag{7}$$

$$\psi = \psi_0 + \varepsilon \, ln\left(\frac{l}{a}\right), \tag{8}$$

where K_c = critical stress intensity factor; E_* = effective modulus of the bi-material system; a = crack length; and $\varepsilon = (1/2\pi) \, ln \, [(1 - \beta) / (1 + \beta)]$. β is one of Dundurs parameters, which represent the mismatch of elastic properties (Dundurs, 1969). l is arbitrary reference length (Rice 1988), and normally 200 μm is used for the interface between cementitious materials (Lim 1996).

The critical stress intensity factor and the effective modulus of the bi-material system can be determined as

$$K_c = YT_c\sqrt{a} \quad \text{and} \tag{9}$$

$$\frac{1}{E_*} = \frac{1}{2}\left[\frac{1}{\overline{E_1}} + \frac{1}{\overline{E_2}}\right] \tag{10}$$

where Y = geometric correction factor; T_c = critical nominal stress occurred at the interface; and

$$\overline{E_i} = E_i / \left(1 - \nu_i\right) \tag{11}$$

for plane strain elastic modulus of material i.

For the symmetric loading in Figure 10,

$$T_c = \frac{P_c}{t}\frac{3B}{2W^2}, \tag{12}$$

$$Y = \sqrt{f_1^2 + (2\varepsilon g_2)^2} \, , \text{ and} \tag{13}$$

$$\psi_0 = arctan\left(\frac{2\varepsilon g_2}{f_1}\right). \tag{14}$$

For the asymmetric loading in Figure 11,

$$T_c = \frac{P_c}{tW}\left[\frac{B-A}{B+A}\right], \tag{15}$$

$$Y = \sqrt{Y_1^2 + Y_2^2} \text{ , and} \qquad (16)$$

$$\psi_0 = arctan\left(\frac{Y_2}{Y_1}\right). \qquad (17)$$

In Equation 12 – 17, P_c is the maximum load, which takes place at the onset of fracture and is obtained from the experiment; t is thickness of the beam at the interface; W is height of the beam; A and B are explained in Figure 10 and also in Figure 11; $Y_1 = (6sf_1 / W) – 2\varepsilon g_1$; $Y_2 = f_2 + 12(s\varepsilon g_2 / W)$; s is the loading offset that is the distance between the interface and the loading line as shown in Figure 11; and f_1, f_2, g_1, and g_2 are the calibration factors given in O'Dowd (1992). By having symmetric as well as asymmetric loading cases, the phase angle can be covered from 0 (mode I, pure tension) to 80 degrees (mixed mode, but mostly shear).

3.2 *Fracture energy measurement*

Fracture energy was measured based on the procedures in the previous section.

Figure 12 shows specimen dimensions. The specimens have a notch of 5 mm height at the interface, and they have a reduced cross section in the middle so as to avoid the unwanted cracks in other locations. The materials are concrete and polymer cement mortar (PCM) to simulate the bi-material interface of a tile structure.

The specimens were fabricated in the following manner. First, the concrete part was cast, and the specimens were cured under water for 28 days and in air for 7 days. The notch was made with a plastic tape, and the interface was roughened with water jet, causing the undulation of the interface to be 0.5 mm at maximum. Next, the PCM part was cast to complete the specimens, and they were cured under water for 28 days. The material properties are shown in Table 3. The Dundurs parameters are calculated with these values.

The phase angles tested in the current study were 0, 30, and 60 degrees. For 0 degree, symmetric loading was applied, and, for 30 and 60 degrees, asymmetric loading was applied. All the loadings were executed under the displacement control of 0.005 mm/sec.

By using the equations in the previous section, interfacial fracture energy is calculated. All the experimental results are plotted in Figure 13. At 0 degree, fracture propagated along the interface. On the other hand, at 30 and 60 degrees, fracture initially propagated along the interface, but in the middle of the interface, it kinked out to PCM. Since the initial fracture was along the interface, these cases can also be considered as interfacial fracture.
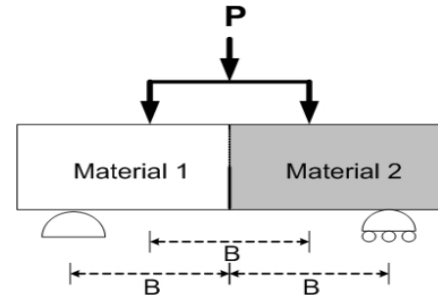
Figure 10. Symmetric four point loading.
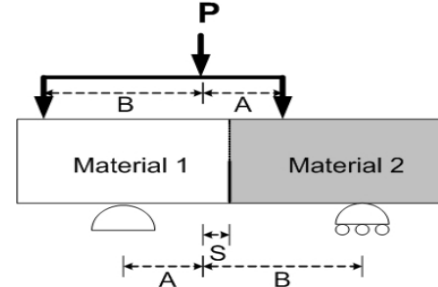
Figure 11. Asymmetric four point loading.
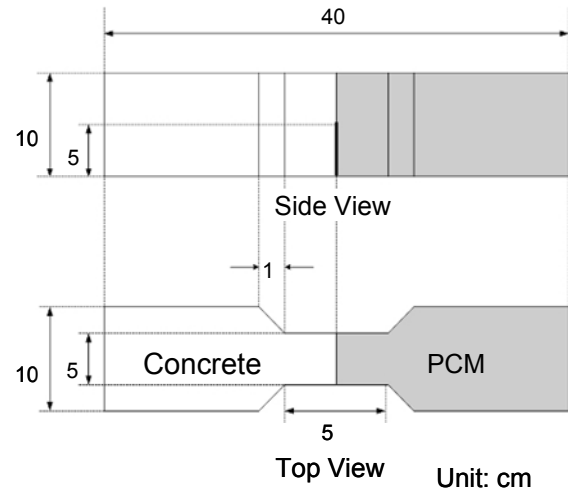
Figure 12. Specimen dimensions.

Table 3. Material properties.

Material	Young's modulus (GPa)	Poisson's ratio
Concrete	30.7	0.207
PCM	21.6	0.212
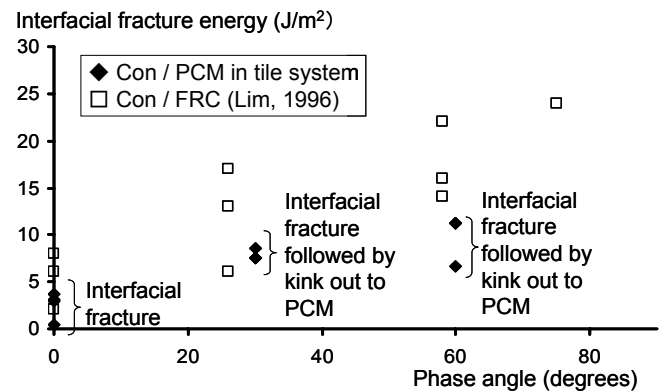
Figure 13. Interfacial fracture energy between concrete and PCM plotted with that between concrete and FRC measured by Lim (1996).

Figure 13 shows the increasing trend of interfacial fracture energy with phase angle. As a reference, the interfacial fracture energy between concrete and fiber reinforced concrete (FRC) is taken from Lim (1996) and plotted together.

For the phase angle from 0 to 60 degrees, the interfacial fracture energy between concrete and PCM was found to vary in the range of 0.5 to 11.2 J/m^2, while Lim (1996) shows that the interfacial fracture energy between concrete and FRC varies in the range of 2 to 24 J/m^2 for the phase angle from 0 to 70 degrees. Although these bi-material systems are different from each other, it can be observed that the interfacial fracture energy of the current system is lower than the one between concrete and FRC, especially at high phase angle.

Based on the fracture energy measurement, finite element analysis is conducted where the interface is modeled with interface elements (Mahaboonpachai & Matsumoto 2005, Mahaboonpachai et al. 2006). Interface element is a four node element with zero thickness, and its constitutive law is defined in normal and shear direction. According to the finite element analysis, the tensile bonding strength is calibrated as 2.5 MPa, and the shear bond strength 5.6 MPa. These values with the thermal stress analysis in the previous section confirm that the interface is subjected more severely to shear stress.

3.3 *Fatigue strength measurement*

Fatigue strength was also measured by testing the specimens of the same dimensions and fabrication processes.

The phase angles are also 0, 30, and 60 degrees. Under either symmetric or asymmetric loading, whichever is appropriate for each angle, fatigue loading was applied under load control at the frequency of 0.1 Hz. The ratio of maximum load to ultimate load was varied from 0.65 to 0.85, where ultimate load had been already obtained in the interfacial fracture energy measurement as P_c. In all the fatigue tests, the ratio of minimum load to maximum load was kept 0.2.

As a result of fatigue tests, S-N diagrams can be obtained, and they are shown in Figure 14, 15, and 16 for the phase angle of 0, 30, and 60 degrees, respectively. Ultimate loads are plotted at 1 cycle, and fatigue life of specimens is plotted in the manner of S-N diagram. In the case of 30 and 60 degrees, one specimen was observed to fail prematurely at 1st cycle of fatigue test. Also, some specimens did not fail before the prescribed number of cycles, and they are labeled with "Not failed" on the plot at the prescribed number of cycles.

Although there are not enough data points to perform a regression analysis, the following two observations can be made generally.

First, the higher the phase angle, the shorter the fatigue life. At the phase angle of 60 degrees, it is seen that the average fatigue life is on the order of 100 cycles for the ratio of 0.8, and 10,000 cycles for 0.7. On the other hand, at 0 degree, fatigue life ranges from 1000 to more than 10,000 cycles, exhibiting a longer fatigue life at higher load level. And, at 60 degrees, fatigue life is possibly shorter than that at 30 degrees. This implies that fatigue strength is weaker under shear dominant loading conditions.
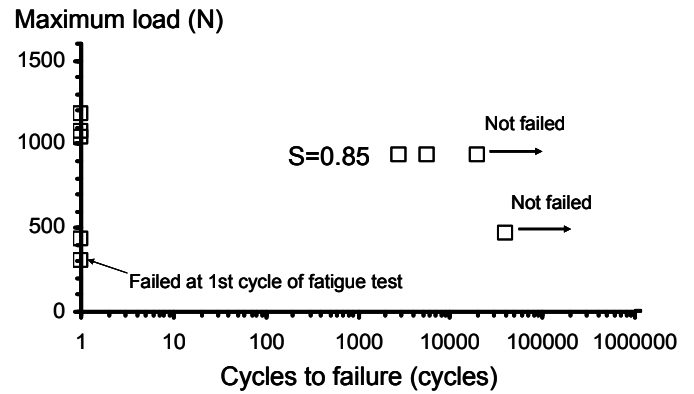
Figure 14. S-N diagram for phase angle = 0 degree.
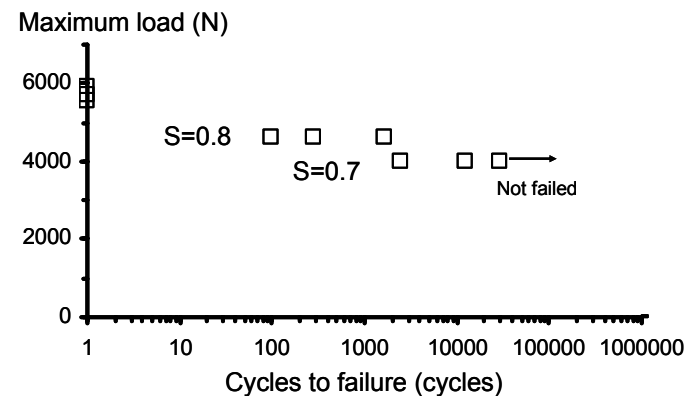
Figure 15. S-N diagram for phase angle = 30 degrees.
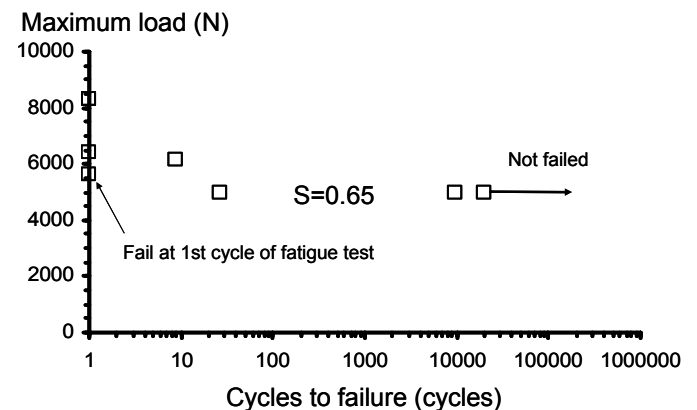
Figure 16. S-N diagram for phase angle = 60 degrees.

Second, although it is considered that bi-material interface is generally a weak location, the S-N diagram of the current system is not significantly different from those of cementitious materials. It is generally observed that fatigue life data points of most cementitious materials lie along a line which connects ultimate load level at 1st cycle and half the ultimate load level at one million cycles. The data points of fatigue life at 30 degrees also lie along this line. Therefore, it can be said that the current bi-material interface has similar fatigue strength characteristics in terms of S-N diagram.

4 CONCLUDING REMARKS

This paper presented preliminary studies for the purposes of understanding the mechanisms of interfacial failure observed in external wall tile structures and achieving the durability of the interface and the tile structures. The studies are conducted from the viewpoints of reaction and resistance of the interface in the tile structure.

For the former part, the temperature measurement in the through-thickness direction has been conducted with a thermography, and the interfacial stresses under thermal loading are estimated with simple analytical models. It estimates the shear stress to be 2.625 MPa and the normal stress in compression 0.008 MPa.

For the latter part, the bi-material interface between concrete and polymer cement mortar was tested to measure interfacial fracture energy and also to measure fatigue strength.

The measurement of interfacial fracture energy shows that, for the phase angle from 0 to 60 degrees, the interfacial fracture energy between concrete and PCM varies from 0.5 to 11.2 J/m^2. The values are smaller than the literature values of the interface between concrete and fiber reinforced concrete, especially at high phase angle.

The interfacial fracture energy was analyzed with finite element analysis in order to obtain the shear and tensile bond strength. The obtained strength values are 5.6 and 2.5 MPa, respectively.

Fatigue strength characteristics of the bi-material interface under different phase angles are summarized in terms of S-N diagrams. The results show that higher phase angle seems to exhibit shorter fatigue life and that the S-N diagram is similar to those of other cementitious materials.

Overall conclusions are as follows. The bi-material interface of a tile structure under thermal loading is subjected more severely to shear stress direction, and the shear stress is on the same order of shear strength. On the other hand, the S-N diagram shows that the interface is not so weak and is comparable to other cementitious materials, while the diagram shows that the interface is slightly shorter life at higher phase angle.

In order to understand the interfacial failure of a tile structure, a finite element analysis is necessary to estimate the interfacial stresses more accurately. The finite element analysis should include the constitutive law of the interface elements in fatigue, and it should conduct the delamination propagation analysis under thermal cyclic loading.

REFERENCES

Dundurs, J. 1969. Edge-bonded dissimilar media. *Journal of Applied Mechanics* 36: 650-652.

Kumagai, T. 1991. Separation failure analysis of ceramic tile applications on external walls. *Journal of Structural and Construction Engineering, Architectural Institute of Japan,* 422: 15-25. (In Japanese)

Kunieda, M., Kurihara, N., Uchida, Y. & Rokugo, K. 2000. Application of tension softening diagrams to evaluation of bond properties at concrete interfaces. *Engineering Fracture Mechanics* 65(2-3): 299-315.

Lim, Y.M. 1996. Interface fracture behavior of rehabilitated concrete infrastructures using engineered cementitious composites. *Ph.d. Thesis.* Ann Arbor: University of Michigan.

Mahaboonpachai, T. & Matsumoto, T. 2005. Investigation of interfacial resistance between concrete and polymer-cement mortar and development of constitutive material model for the interface. *Journal of Applied Mechanics, Japan Society of Civil Engineers* 8: 977-985.

Mahaboonpachai, T., Inaba, Y. & Matsumoto, T. 2006. Investigation of interfacial resistance of the interface between concrete and polymer–cement mortar in tile applications. *Proceedings of the second international conference on structural health monitoring of intelligent infrastructure, Shenzhen, 16-18 November, 2005,* 2: 1481-1487.

O'Dowd, N.P., Shih, C.F. & Stout, M.G. 1992. Testing geometry for measuring interfacial toughness. *International Journal of Solids and Structures* 29(5): 571-589.

Rice, J.R. 1988. Elastic fracture concepts for interfacial cracks. *Journal of Applied Mechanics* 55: 98-103.

Rumbayan, R., Mahaboonpachai, T. & Matsumoto, T. 2006. Thermographic measurement and thermal stress analysis at the interface of external wall tile structure. *Journal of Applied Mechanics, Japan Society of Civil Engineers*, 9: 1069-1076.